Semiconductor Science and Technology

PAPER

Fabrication and characterization of Au/n-type InP Schottky barrier diode with monolayer graphene interlayer

To cite this article: Fulya Esra Cimilli Çatr 2020 *Semicond. Sci. Technol.* **35** 035023

View the article online for updates and enhancements.



IOP ebooks™

Bringing you innovative digital publishing with leading voices to create your essential collection of books in STEM research.

Start exploring the collection - download the first chapter of every title for free.

This content was downloaded from IP address 148.253.213.132 on 28/02/2020 at 09:49

IOP Publishing Semiconductor Science and Technology
Semicond. Sci. Technol. **35** (2020) 035023 (9pp) https://doi.org/10.1088/1361-6641/ab6bb4

Fabrication and characterization of Au/n-type InP Schottky barrier diode with monolayer graphene interlayer

Fulya Esra Cimilli Çatır

Erzincan Binali Yildirim University, Vocational School, Department of Electronic Technologies, 24200, Erzincan, Turkey

E-mail: fcatir@erzincan.edu.tr

Received 2 October 2019, revised 7 November 2019
Accepted for publication 14 January 2020
Published 19 February 2020

Abstract

Au/graphene/n-InP Schottky barrier diode (SBD) was fabricated by the use of spray pyrolysis technique with a monolayer graphene interlayer, and the temperature dependent characteristics was performed in a wide temperature range from 60 to 300 K with steps. The Au/GR/n-InP SBD exhibited excellent rectifying behavior however barrier height (Φ_{b0}) of the device increased with increasing temperature while ideality factor (n) and series resistance (R_s) decreased. The strong temperature dependency of SBH and the deviation from theoretical value of Richardson constant clarified by considering a Gaussian distribution model of the SBH which was caused by the BH inhomogeneities. The mean BH $\overline{\Phi}_{b0}$ of 0.94 and 0.59 eV was estimated with the standard deviation of 0.011 and 0.004 eV attributed to the presence of a double GD of SBD. The modified Richardson plots gave mean BH value of 0.98 and 0.70 eV and the Richardson constant values of 8.10, 13,38 A K^{-2} cm^{-2} was very close to its theoretical value of 9.4 A K^{-2} cm^{-2}. These results yields that carrier transport mechanism of Au/GR/n-InP SBD can be clarified by Thermionic-emission-diffusion (TED) mechanism with a double Gaussian distribution of the SBHs. In addition, the I–V characteristics of SBD under dark and light ambiance indicates that Au/graphene/n-InP is strongly dependent on the light effect. Thus, we can conclude that graphene/n-InP device is a potential candidate for photovoltaic systems. Moreover, the UV–vis spectroscopy of the graphene film exhibit a strong absorption as $A = 9.45\%$ compared to the literature, that is, Au/GR/n-InP SBD grown by spray pyrolysis has excellent optical properties for optoelectronic applications.

Keywords: graphene, 2D materials, Schottky barrier diode, InP, absorbance

(Some figures may appear in colour only in the online journal)

Introduction

Graphene consists of a single layer of graphite and shows very attractive mechanical, optical and electronic properties [1–4]. Graphene electrons are easy to pass through the material without much effort, and in this case graphene has enormous electron mobility. It has a high carrier concentration and mobility that allows an electric current to flow rapidly at a speed approaching the speed of light (the carrier mobility is over 200 000 cm^2 V^{-1} s^{-1} [5]). This is a very high mobility compared to copper and silicon semiconductors used today. So its electron transport properties are unique. Today, silicon-based electronic technology is very close to its theoretical limits due to the structural properties of silicon. Therefore, graphene-based materials are likely to shape the electronic technology of the future and graphene is shown as the wonderful material of the future. Graphene is the strongest candidate for transparent, touchable, foldable displays due to its combination of light transmittance (almost 98% [5]), mechanical strength and electrical conductivity. It is also intended to be used in areas such as sensors, solar cells, light panels [2, 6]. If the application of graphene in technological

 © 2020 IOP Publishing Ltd Printed in the UK

fields is improved, it will allow data used in devices such as touch screens, computers and mobile phones to be transmitted at much higher speeds.

Many methods can be used for chemical graphene deposition [7] using gas precursors or liquid precursors. The most commonly used method to grow graphene is chemical vapor deposition (CVD) technique [3, 7] which reveals advantages for growing especially large area and high quality graphene films [8]. Spray pyrolysis technique (SPT) is the simple and low cost film deposition process as a good technique for an altered method of CVD. This method is used in technological applications, especially in the production of photovoltaic solar cells. It has gained importance with its successful use in precipitation of semiconductor layers. Therefore, interest in obtaining film by spray pyrolysis method is increasing. In addition it is a well-known technique to grow nanoparticles and thin films homogeneously [9].

On the other hand, metal-graphene contact is a very active subject of current study, and the physical mechanisms behind it are not completely understood [2, 10]. Due to the potential of graphene to be used in technological applications, this scientific interest in Graphene has made it the most active research subject of recent years. Graphene transistors have been extensively studied for a long time, as a result of which an understanding of the physical and manufacturing techniques of a graphene Schottky contact is still in its infancy [11]. As Pathak *et al* [2] indicated, the fundamental transport mechanism of graphene based Schottky diodes is not properly understood. Within this context, electrical and electronic properties of metal semiconductor contacts prepared with graphene structures will be examined by using Thermionic Emission (TE), activation energy plots, and barrier inhomogeneity model based on the current–voltage–temperature (*I–V–T*) characteristics of Au/graphene/n-InP/In structures. The Raman Spectrum, SEM images, and the UV–vis spectrum of graphene films investigated and possible applicability of Au/graphene/n-InP/In structures in electronic technology was investigated.

Experimental

The Au/InP SBDs structure used in this study were fabricated using n-type single crystals n-InP wafer with (100) surface orientation, 1.5×10^{16} cm^{-3} carrier concentration (N_D) (given by the manufacturer). Before the SBD fabrication process, n-InP wafer was degreased for 5 min which is carried out consecutively using ultrasonic agitation in organic solvent of trichloroethylene ($CHClCCl_2$), acetone (CH_3COCH_3) and methyl alcohol (CH_3OH), etched in H_2SO_4:H_2O_2:H_2O (5:1:1) within 1 min to remove the impurities and surfaces damages. Finally plunged in de-ionized water of resistivity of 18 MΩ cm for a prolonged time. During to each cleaning step, the wafer was rinsed with de-ionized water. After surface cleaning of n-InP, high purity (99.9%) In was coated with thickness control integrated NANOVAK NVTH-350 thermal evaporation system at a pressure about 10^{-6} mbar in high vacuum system with 200 nm thickness. To perform the ohmic contact, n-InP wafer was annealed at 300 °C for 3 min under a N_2 gas flow. In addition, glass substrates were ultrasonically cleaned with acetone (CH_3COCH_3), methyl alcohol (CH_3OH) and de-ionized water. Then they were subjected to pre-heating at 700 °C. After providing ohmic contacts, to obtain graphene interfacial layer between metal–semiconductor (M/S), graphene (GR) nano powder (SSA: 150 g cm^{-2}, purity: 99.5%) was supplied from a chemical industry in production of carbon based materials. GR was deposited on the other side of the n-InP and the glass substrates by spray pyrolysis technique using dispersed solution of graphene. Holmarc's HD-TH-04 Spray Pyrolysis system of thin film magnifying device used in chemical spraying method. GR solution (0.1 M) in *N*, *N*-dimethylformamide (DMF), used as solvent of this solution, was prepared utilizing ultrasonic vibration for 48 h. The solution flow rate was 5 ml min^{-1} and the distance between nozzle and substrate was 20 cm. The heater of spray pyrolysis system was set 200 °C in order to obtain uniform thin films. After film depositing the graphene films were dried at 50° under nitrogen gas for 48 h. Depending on the Raman Spectra of graphene film shown in figure 1, the graphene film was found to be a monolayer so the thickness of the graphene film is estimated to be 0.345 nm [12, 13]. Then the Schottky diodes were fabricated by using Au (99.9% purity) metal deposited on the graphene for enhanced current spreading. The circular pattern of the Schottky contact with a diameter of 0.5 mm and 300 nm thickness was obtained by thickness control integrated NANOVAK NVTH-350 thermal evaporation system under 10^{-6} mbar vacuum conditions. The surface morphology was characterized by Raman Spectroscopy and SEM. The optical absorption was performed using a Perkin–Elmer Lambda 2 S UV–vis. spectrophotometer (190–1100 nm).

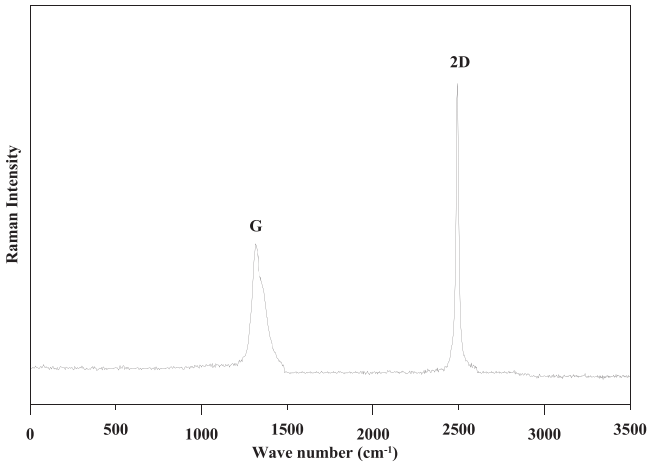


Figure 1. The Raman Spectroscopy of mono-layered graphene film.

I–V–T measurements for the Au/GR/n-InP/In diodes were made using a closed-cycle He cryostat with 20 K temperature steps at 60 K to 300 K temperature range. By using a LakeShore 330 temperature controller. The current–voltage–temperature (*I–V–T*) characteristics of Au/GR/n-InP/In SBDs were measured with a Keithley 2400 and a 6514 Keithley electrometer.

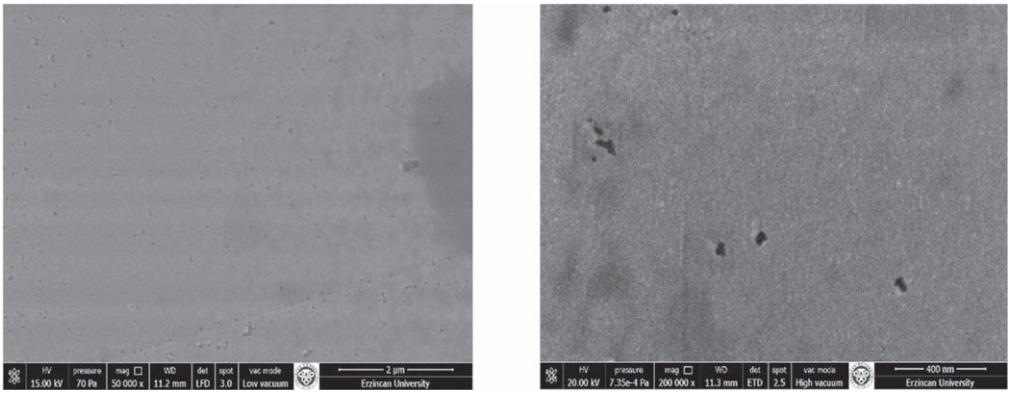


Figure 2. SEM images of the GR/InP Schottky diode (top view).

Results and discussion

Raman spectroscopy is the perfect and non-destructive technique to analyze the single, double, few or multi-layer graphene films [14] and other carbon-based materials. The most important properties of the Raman spectrum of graphene are: D-peak at 1350 cm^{-1}, G-peak at 1580 cm^{-1}, and 2D-peak at ~2700 cm^{-1} [15]. These three basic elements play an important role in distinguishing the number of layers and quality of graphene film from the Raman spectrum. The first of these; the decrease in the G-peak intensity in the monolayer graphene and the change in the shape of the 2D-peak. For monolayer graphene, the 2D-peak gives a sharper and narrower peak, whereas for multilayer graphene, the shape of the 2D peak expands and begins to deteriorate. The last is that the D-peak becomes prominent in defective structures. So, the number of microscopic defects in graphene can be determined by the intensity of the D-peak [16]. The perfect graphene spectrum does not have a D-peak [17].

The D-peak may also result from some factors such as chemical doping of the graphene film and the grain boundaries. If the density ratio of the D and G-peaks does not exceed 0,1 value, the graphene film is of suitable quality. Figure 1 shows the Raman spectroscopy of as-prepared graphene film. The absence of D-peak around 1350 cm^{-1} reveals that the defect density of synthesized graphene film is low and high-quality graphene layers were produced [17]. In addition, the integrated intensity ratio found as $I_G/I_{2D} \cong 2$ which indicates that the graphene film on InP substrate was a monolayer, and it is in good agreement with the values reported in previous reports [14, 18].

The SEM images of graphene film grown directly on n-InP semiconductor substrate by Spray Pyrolysis method is given in figure 2 and it is seen that the film grows homogeneously on the surface and completely covers the surface and there are gaps in some parts. The light and dark areas in the images are caused by electron signals from different regions.

Figure 3 shows the *I–V* characteristics of Au/n type InP SBDs with and without graphene interlayer at room temperature. It is evident that both devices exhibit good rectifier properties because the forward bias current shows an exponential increase while reverse bias current shows slightly voltage dependence. According to the TE theory, the current through Schottky contact at a biasvoltage $V \gg 3kT/q$ is given as [19]:

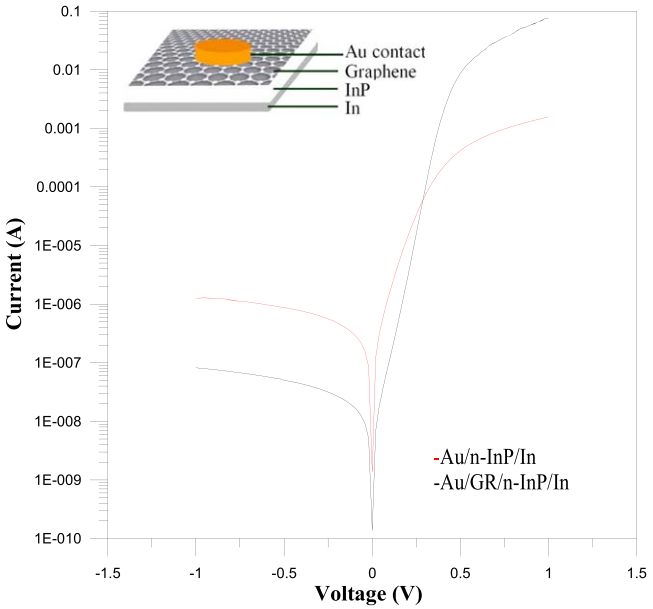


Figure 3. Semi-log *I–V* characteristics of as-dep. and Au/GR/n-InP Schottky diode (300 K).

$$I = I_0 \exp\left(\frac{qV}{nkT}\right)\left[1 - \exp\left(-\frac{qV}{kT}\right)\right], \quad (1)$$

where I_0 is the saturation current derived from ln*I–V* plot and given by

$$I_0 = A\,A^{*}T^{2} \exp\left(-\frac{q\Phi_{b0}}{kT}\right) \quad (2)$$

A is the Schottky contact area, k is the Boltzmann constant, A^* is the effective Richardson constant and 9.8 A cm^{-2} K^{-2} for

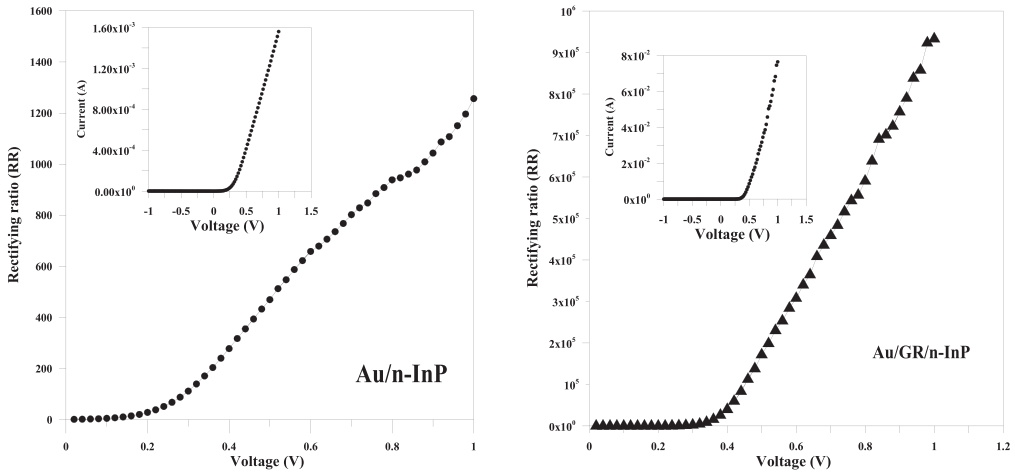


Figure 4. Rectifying ratio-voltage plots calculated from current–voltage characteristics of Au/n-InP and Au/GR/n-InP Schottky diodes at room temperature (300 K).

n-type InP [19], Φ_{b0} is the zero bias barrier height (BH), n is the ideality factor and T is the temperature value in kelvin.

The ideality factor can be obtained from the forward bias ln$I$–V characteristics by:

$$n = \frac{q}{kT}\left(\frac{dV}{d\ \ln I}\right) \tag{3}$$

The effective barrier height of Φ_{b0} can be determined from equation (2) and given as:

$$\Phi_{b0} = \frac{kT}{q}\ln\left(\frac{AA^{*}T^{2}}{I_0}\right) \tag{4}$$

The values of n and Φ_{b0} are calculated for as-dep. and graphene /n-InP Schottky diodes at 300 K found to be 1.34–0.67 eV and 1.07–0.77 eV, respectively. Both devices exhibited a deviating from the unity of the ideality factor and this could be attributed to the presence of a wide distribution of low SB patches due to a laterally inhomogeneous barrier height [20]. In addition, it is noted that the barrier height of graphene/n-InP SBD was quite higher than the SBD without graphene, indicating that the graphene interlayer predominately affected the interfacial potantial barrier of the Au/n-InP Schottky contact.

The series resistance (R_s) of Au/GR/n-InP and Au/n-InP was calculated by using the method developed by Cheungs [21], R_s values values were found to be 5.29 Ω and 22.21 Ω from experimental forward bias I–V characteristics at room temperature (300 K). As a result, it is seen that graphene interface greatly decreases series resistance value of Au/n-InP diode.

The rectifying ratio (RR) was calculated from the ratio of forward and reverse current at a constant V value by using equation $RR = |I_f|/|I_r|$. The RR of Au/GR/n-InP and Au/n-InP was about 1.71×10^5 and 4.63×10^2 at ±0.5 V, respectively. The RR value of diode with graphene film was increased by about 369 times compared to the diode with non-interface and it can be attributed to the graphene film which reduces leakage current and shunt resistance increase (Rsh) of the Au/GR/n-InP Schottky diode [22]. Furthermore, the rectifying ratio-voltage characteristics of the Au/n-InP and Au/GR/n-InP diodes at ±1 V voltage range was calculated and plotted in figure 4. As can be seen in figure 4, the RR values increases with the increasing bias voltage [23] and the RR increased in the order of 10^3 between the diodes with and without graphene interlayer consistent with the literature [24].

In recent years, there have been many scientific studies suggested that it is possible to control the barrier height (BH), decrease the series resistance (Rs) and increase the rectification by using interfacial layers such as graphene [25]. In this study, from the characteristic parameters of the Au/GR/n-InP diode calculated at room temperature (300 K), it is seen that the barrier height increased, the ideality decreased, the series resistance decreased and the rectification ratio highly increased compared to Au/n-InP diode. Thus, a great increase in the quality of the diode has been determined due to the graphene interface.

Schottky diodes also play important roles in electronic devices such as infrared detectors operating at very low temperatures, sensors in thermal imaging, microwave diodes, infrared and nuclear particle detectors [26]. Moreover, metal-graphene contact is a very active subject and to understand the physical mechanisms behind it, the analysis of the I–V characteristics of Schottky diodes only at room temperatures does not provide sufficient information about the nature of the barrier formation or their transport mechanism. Therefore, the I–V characteristics of the Au/graphene/n-InP/In SBD for temperature range 60–300 K is measured and presented in figure 5. The n and Φ_{b0} were calculated by equations (3)–(4) and shown in table 1. The n and Φ_{b0} range from 1.07–0.77 eV for 300 K and 6.85–0.20 eV for 60 K, respectively The variation of ideality factor, especially $n > 1$, attributed to the existence of interface states and the spatial barrier inhomogeneties at the metal–semiconductor (MS) interface [27]. In addition, in figure 5. I–V curves demonstrates deviation from linearity towards higher bias voltage values. This indicates the prescence of series resistance (R_s) and using the method developed by Cheungs [21], R_s values are calculated as a

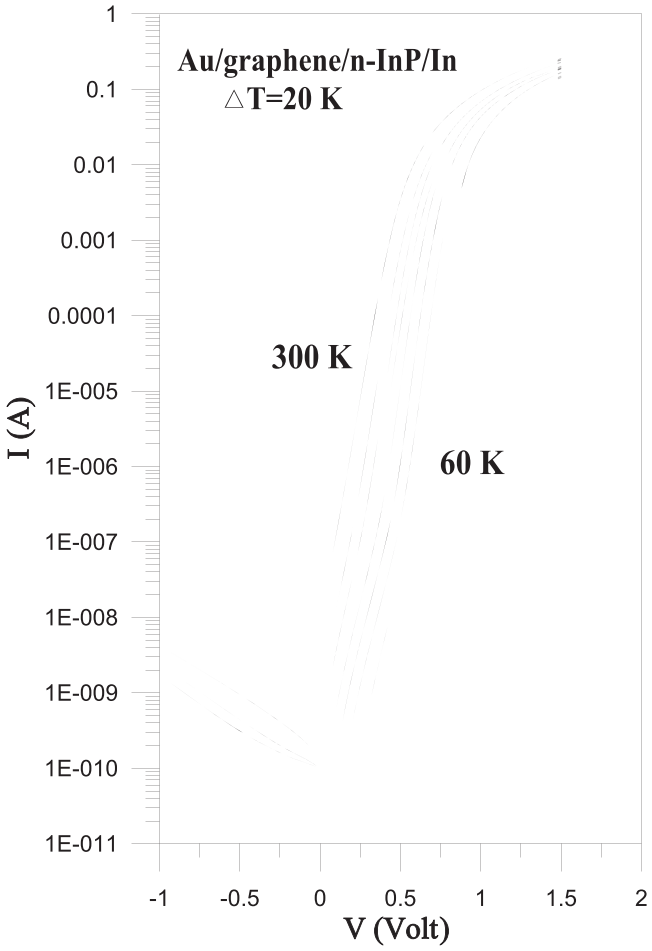


Figure 5. Semi-log *I–V* characteristics of Au/GR/n-InP Schottky diode as a function of temperature (60–300 K).

Table 1. Temperature dependent characteristic parameters of Au/GR/n-InP Schottky diode calculated from *I–V–T* measurements.

T (K)	n	Φ_b (eV)	R_s (Ω) $dV/dlnI$	R_s (Ω) $H(I)/I$
300	1.070	0.774	5.104	5.470
280	1.174	0.719	5.025	5.243
260	1.262	0.713	5.231	5.428
240	1.227	0.687	5.497	5.556
220	1.277	0.634	5.844	5.850
200	1.557	0.600	6.035	6.129
180	2.557	0.540	6.194	6.367
160	2.533	0.492	6.411	6.670
140	2.114	0.466	6.886	7.240
120	3.349	0.402	7.135	7.948
100	3.954	0.343	7.378	8.849
80	5.085	0.273	7.804	10.065
60	6.848	0.201	8.219	10.822

function of temperature from experimental forward bias *I–V* characteristics and shown in both figure 6(b) and table 1.

As shown in figure 6(b) and table 1, series resistance values increase with decreasing temperature. The series resistance values (R_s) for 300 K and 60 K were obtained as 5.10 Ω and 5.47 Ω for 300 K and 8.22 Ω and 10.82 Ω for 60 K, respectively. Increased series resistance (R_s) values with decreasing temperature may be caused by decreasing free carrier density at low temperatures or increasing the ideality factor value of the diode [28]. The temperature-dependent variation of n and Φ_{b0} is shown in figure 6(a). As shown in figure 6(a) and table 1, the values of the n and Φ_{b0} are temperature dependent and ideality factor decrease properly with increasing temperature and potential barrier height increase with increasing temperature. Since the ideality factor and the barrier height have strong temperature dependence, they exhibit an unusual behavior.

The Richardson plots gives more information about the spatial distribution of the barrier height. Consequently, the current in equation (2) can rewritten as:

$$\ln\left(\frac{I_0}{T^2}\right) = \ln(AA^*) - \frac{q\Phi_{b0}}{kT} \tag{5}$$

According to equation (4), if the Schottky barrier is independent of the temperature, the change of $\ln(I_0/T^2) - 1/kT$ or $1/nkT$ should be linear and from these equations. The graphs of $\ln(I_0/T^2)/-1/kT$ or $1/nkT$ are plotted at. Figure 7. Hence, the zero bias barrier height (Φ_{b0}) value was found to be 0.74 eV. However, it deviates from linearity at low temperatures as seen in figure 7. Also it indicates that the SBH is strongly dependent on the temperature. The deviation in Richardson curves may be due to non-homogeneous barrier heights (BHs) and potential variations at the interface with low and high barrier areas. At low temperatures, electrons can pass over the lower barriers and the current transport is by flowing through the patches that have lower SBH [29]. When the temperature increases much more electrons have the enough energy to surpass the higher barrier and consequently the apparent barrier height increases with the increasing voltage and temperature [30, 31]. The nonlinearity in Richardson curves at low temperatures can be explained using the modified Richardson equation together with Gaussian distributed barrier height model. All these results show that there is a significant deviation in current-transmission from the ideal thermionic-emission (TE) theory. Therefore, the causes of the deviation in the forward bias *I–V* characteristics were investigated and it was concluded that there is a barrier inhomogeneity between metal and semiconductor.

In particular at low temperatures, the decrease of zero bias barrier height and the increase of ideality factor may be caused by barrier height inhomogeneities derived from the differences in thickness and formation of the interface layer, non-uniformity of interfacial charges, introduced by Song et al as first [32]. In order to describe them, one of the models explaining deviations from the ideal state in Schottky diode is 'the barrier inhomogeneity model'. The behavior in this case can be derived by using Gaussian distribution. In the literature barrier inhomogeneity has been explained by many current-transmission mechanisms (such as thermionic field emission, field emission or multi-layer tunneling). But it is clear that these explanations are not sufficient.

Abnormal increases in the ideality factor, especially at low temperatures, cannot be explained only by the thickness of the interface layer or the presence of the interface states.

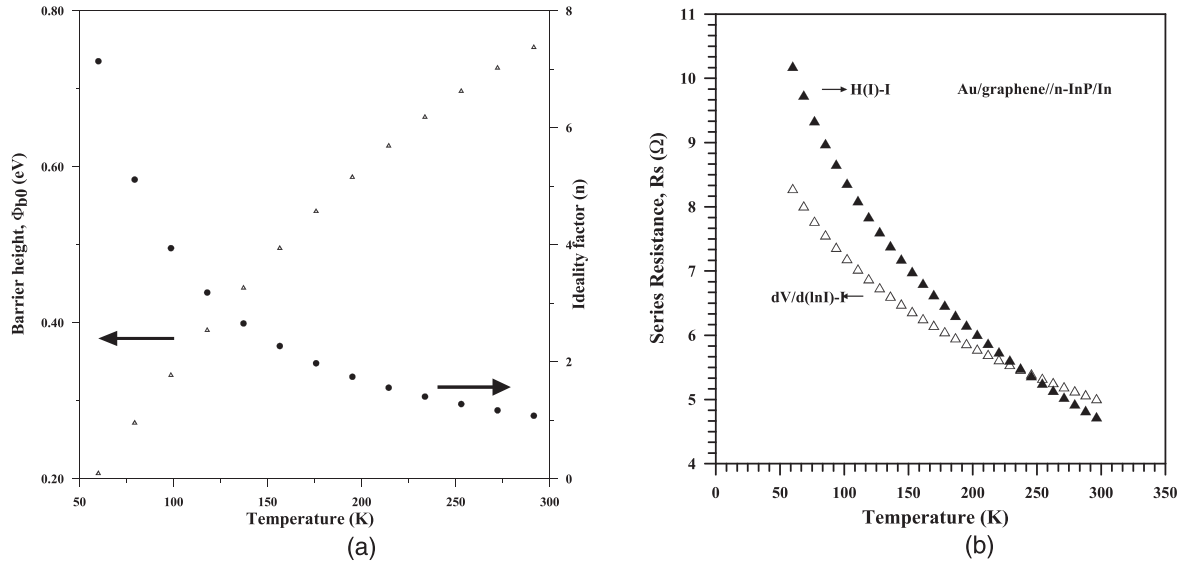


Figure 6. (a) Barrier height (Φ_{b0}) and ideality factor (n) (b) Series resistance of Au/GR/n-InP Schottky diode as a function of temperature (60–300 K).

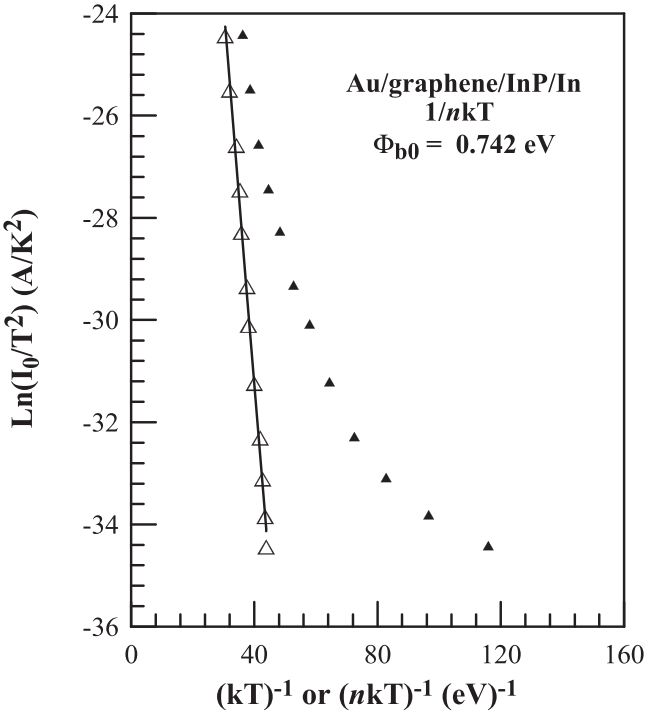


Figure 7. The Richardson plot ($\ln(I_0/T^2)$ versus $1/kT$ or $1/nkT$ variation) for Au/GR/n-InP Schottky diode.

Gaussian distribution function is the most preferred method for explaining abnormal properties of Schottky barrier diodes especially at low temperatures. Gaussian distribution expression for a Schoty diode with an average barrier height and standard deviation given as:

$$P(\Phi_{ap}) = \frac{1}{\sigma_s\sqrt{2\pi}}\exp\left(-\frac{(\Phi_{ap} - \bar{\Phi}_{b0})^2}{2\sigma_s^2}\right) \quad (6)$$

Here, $\frac{1}{\sigma_s\sqrt{2\pi}}$ is the normalization constant of the Gauss barrier height distribution. Total current in the forward bias of a

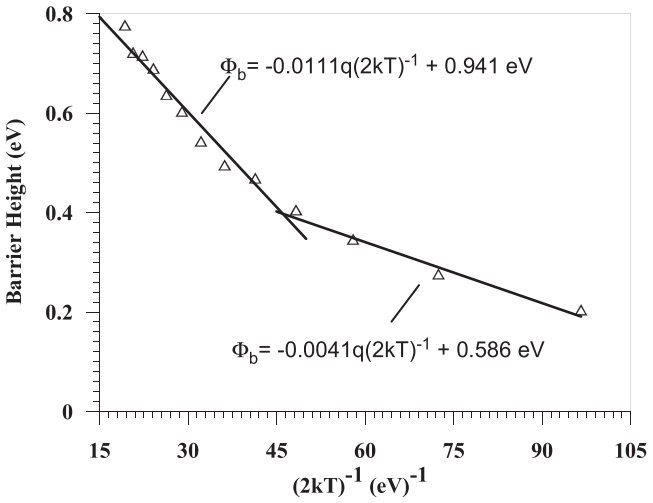


Figure 8. The apparent barrier height (Φ_{ap}) versus $q/2kT$ graph for Au/GR/n-InP Schottky diode.

Schottky diode that comprise barrier inhomogeneities can be expressed as:

$$I(V) = \int_{-\infty}^{+\infty} I(\Phi_{ap}, V)P(\Phi_{ap})d\Phi_{ap} \quad (7)$$

where $I(\Phi_{ap},V)$ is the current for a BH at a V bias based on thermionic emission-diffusion (TED) theory and $P(\Phi_{ap})$ is the probability of trueness for the BH. Which is called normalization distribution function. Φ_{ap} is the apparent barrier height is given by:

$$\Phi_{ap} = \overline{\Phi}_{b0} - \frac{q\sigma_s^2}{2kT} \quad (8)$$

Here, $\overline{\Phi}_{b0}$ is the mean Schottky barrier height and σ_s is the standard deviation at zero bias voltage. Experimental $\Phi_{ap}-q/2kT$ curves are given in figure 8 to explain the Gaussian distribution for barrier height. $\overline{\Phi}_{b0}$ was estimated as 0.94 and 0.59 eV, and the σ_s was determined to be 0.011 and

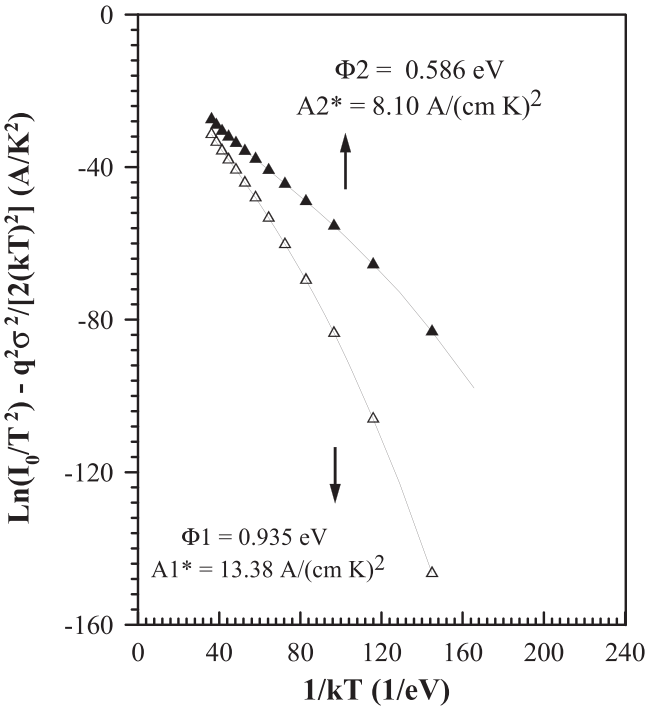


Figure 9. The modified Richardson curves ($\ln(I_0/T^2)-(q\sigma_s^2/2k^2T^2)$ versus q/kT variation) plot for Au/GR/n-InP/In Schottky diode according to GD of BHs.

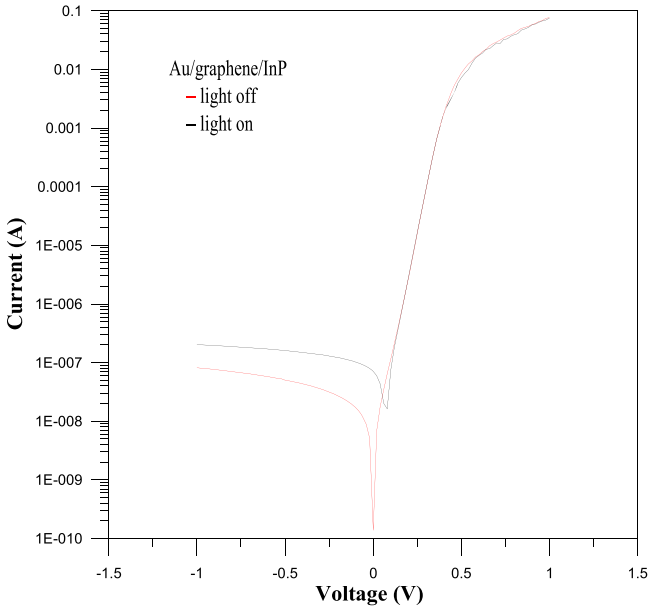


Figure 10. Semi-log *I–V* characteristics of graphene/n-InP Schottky diode under dark and daylight ambience (300 K).

0.004 eV. The lower values of σ_s are the fact that there is lower inhomogeneous barrier distribution. Figure 8 show a double slope structure as low temperatures region and high temperatures region that suits the barrier inhomogeneity model of Schottky contacts and the double Gaussian distribution of the SBHs [33].

These experimental results show that the current-transmission mechanism of Au/GR/n-InP/In Schottky diodes can be used to successfully generate non-homogeneous BHs in a wide temperature range according to the Thermionic-emission-diffusion (TED) mechanism using Gaussian distribution function. Furthermore, the series resistance value plays an important role in the deviation from the linearity in direct voltage ln*I–V* curves at forward voltage values. R_s values decrease with increasing temperature in accordance with the literature.

As seen in figure 7, conventional activation energy $\ln(I_0/T^2)$ graphs according to $1/kT$ deviates from linearity at low temperatures. To explain this discrepancy, equation (5) is rearranged according to Gaussian distribution of barrier height and given as:

$$\ln\left(\frac{I_0}{T^2}\right)-\left(\frac{q^2\sigma_s^2}{2k^2T^2}\right)=\ln(AA^*)-\frac{q\overline{\Phi}_{b0}}{kT} \tag{9}$$

The modified Richardson curves of $\ln(I_0/T^2)-(q\sigma_s^2/2k^2T^2)$ versus q/kT variation plot for Au/GR/n-InP/In Schottky diode is presented in figure 9 according to GD of BHs. The slope of this graph gives $\overline{\Phi}_{b0}$ directly. The average barrier height found here is $\overline{\Phi}_{b0}$=0.98 eV and $\overline{\Phi}_{b0}$=0.70 eV. Moreover, the Richardson constant $A^* = 8.10\ \mathrm{A\,K^{-2}\,cm^{-2}}$ $A^* = 13.38\ \mathrm{A\,K^{-2}\,cm^{-2}}$ were found using the fit equation of this graph. These values of A^* is very close to its theoretical value and the difference of the Richardson constant values from the known value of $9.4\ \mathrm{A\,K^{-2}\,cm^{-2}}$ can be explained by the potential fluctuations in the interface consisting of low and high disability areas and the inhomogeneous barrier height. These experimental results for the Au/GR/n-InP SBD are consistent with the temperature-dependent Gaussian barrier height distribution model. That is, with such a model, it can be explained why the ideality factor is high than unity and that the barrier height increases with increasing temperature [33].

Figure 10 compares the room-temperature *I–V* curves of the graphene/n-InP Schottky diode obtained in darkness and at daylight ambiance. The forward current remains unchanged, while the reverse current increases. This means that, the reverse Schottky current was found to be quite dependent on the light effect, which is attributed to the increase in carrier intensity at the interface. That is, the increase in current is caused by the increase in electron and hole pairs due to the effect of light. As a result, the Au/GR/n-InP/In Schottky diode shows photovoltaic properties and it can be used as a circuit element in light sensitive electronic circuit systems.

Graphene has a gapless energy band that allows charge carrier generation with light absorption in a wide spectrum of energy so it has high interest optical properties for optoelectronic applications [11].

When the absorption-wavelength graph is examined (figure 11), it is seen that the graphene film absorbs the rays of the wavelength at about 260–350 nm vigorously and transmit the rays of the other wavelengths. As seen in figure 11, the graphene absorption spectrum exhibits a maximum absorption peak at about 270 nm attributed to the π–π^* transition of the aromatic C–C ring of graphene sheets, in consistency with earlier reports [34–36]. Zhu *et al* indicated that the monolayer graphene has a narrower UV absorption band with high

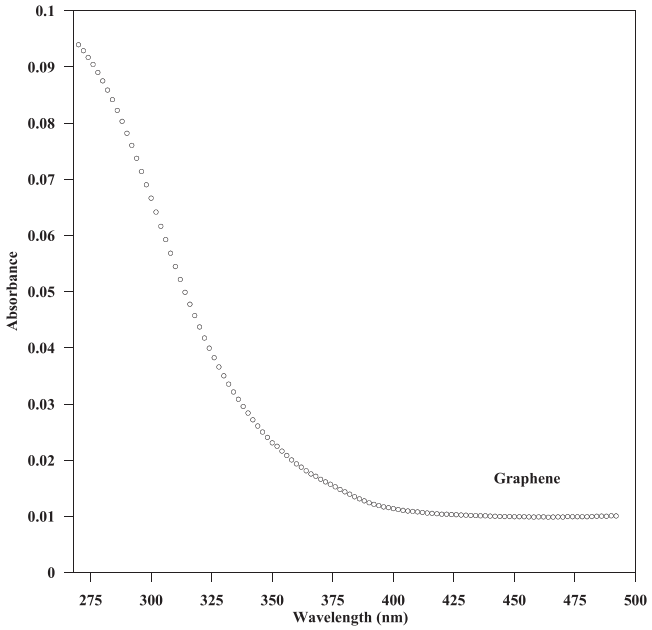


Figure 11. The UV–visible absorption spectra of the graphene film.

suppression of visible absorption [34], based on this statement, at figure 11 the UV–visible absorption spectra of the graphene film which was grown on n-InP substrate is in good agreement with this remark and we can conclude that it is a manolayer graphene film as calculated from Raman spectrum. As seen in figure 11, the graphene film exhibit a strong absorption as $A = 9.45\%$ compared to the given in the literature [36]. Therefore, we can conclude that Au/GR/n-InP SBD grown by spray pyrolysis method has excellent optical properties for optoelectronic applications.

Conclusion

In conclusion, the monolayer graphene obtained by spray pyrolysis method as the interlayer in Au/n-type InP SBD was employed. The temperature dependent performance of Au/GR/n-InP/In SBD diode has been demonstrated in a wide range of 60–300 K. The electrical and optical characteristics and carrier transport mechanism and the morphological properties of graphene/InP Schottky contacts have been analyzed in detail. The Au/GR/n-InP SBD exhibited excellent rectifying behavior in contrast to the Au/n-InP diode. The barrier height values increase with increasing temperature while ideality factor and series resistance values decrease. The strong temperature dependency of SBHs and the deviation from theoretical value of Richardson constant demonstrates the presence of barrier inhomogeneity of SBD. To clarify this inconsistency, double Gaussian distribution model of the SBH applied to the *I–V–T* data of Au/GR/n-InP SBD and the mean BH $\overline{\Phi}_{b0}$ of 0.94 eV and 0.59 eV was estimated with the standard deviation of 0.011 and 0.004 eV. The modified activation energy curves yielded mean BH value of $\overline{\Phi}_{b0} = 0.98$ eV and $\overline{\Phi}_{b0} = 0.70$ eV and the Richardson constant values of $A^* = 8.10\ \mathrm{A\,K^{-2}\,cm^{-2}}$ and $A^{**} = 13.38\ \mathrm{A\,K^{-2}\,cm^{-2}}$ was very close to its theoretical value. Considering all this, we come to a decision that carrier transport mechanism of Au/GR/n-InP SBD can be clarified by TE mechanism with a double Gaussian distribution of the SBHs. In addition, the *I–V* characteristics of graphene/n-InP SBD under dark and light showed that the reverse Schottky current was found to be quite dependent on the light effect. Such a result indicates that graphene/n-InP is a potential applicant for photovoltaic systems. Also the graphene absorption spectrum showed a sharp peak at 270 nm indicates a monolayer graphene similar to that obtained from Raman spectroscopy. This monolayer graphene film exhibit a strong absorption as $A = 9.45\%$ consistent with the literature. Thus, we can conclude that Au/GR/n-InP SBD has excellent optical properties for optoelectronic applications.

ORCID iDs

Fulya Esra Cimilli Çatır https://orcid.org/0000-0002-0757-3130

References

[1] Haditale M, Zabihipour A and Koppelaar H 2018 A comparison of I–V characteristics of graphene silicon and graphene-porous silicon hybrid structures *Superlattices Microstruct.* **122** 387–93
[2] Pathak C S *et al* 2018 Current transport properties of monolayer graphene/n-si Schottky diodes *Semicond. Sci. Technol.* **33** 055006
[3] Rehman M A *et al* 2018 Influence of an Al2O3 interlayer in a directly grown graphene-silicon Schottky junction solar cell *Carbon* **132** 157–64
[4] Çiçek O *et al* 2017 Synthesis and characterization of pure and graphene (Gr)-doped organic/polymer nanocomposites to investigate the electrical and photoconductivity properties of Au/n-GaAs structures *Composites* B **113** 14–23
[5] Kalita G *et al* 2018 Schottky barrier diode characteristics of graphene-gan heterojunction with hexagonal boron nitride interfacial layer *Phys. Status Solidi* a **215** 1800089
[6] 2010 Nobel Prize award (www.nobelprize.org/uploads/2018/06/popular-physicsprize2010.pdf)
[7] Shi Z and Jayatissa A H 2017 The impact of graphene on the fabrication of thin film solar cells: current status and future prospects *Materials* **11** 36
[8] Li Z 2017 Ultrasonic spray pyrolysis method for graphene films synthesis *Acta Tech.* **62** 1–8
[9] AlShammari A *et al* 2018 Growth and structural properties of graphene oxide thin film with spray pyrolysis technique *IOP Conf. Ser.: Mater. Sci. Eng.* **409** 012007
[10] Khurelbaatar Z *et al* 2014 Modification of Schottky barrier properties of Au/n-type Ge Schottky barrier diode using monolayer graphene interlayer *J. Alloys Compd.* **614** 323–9
[11] Di Bartolomeo A 2016 Graphene Schottky diodes: An experimental review of the rectifying graphene/semiconductor heterojunction *Phys. Rep.* **606** 1–58
[12] Mohammed M *et al* 2012 Junction investigation of graphene/silicon Schottky diodes *Nanoscale Res. Lett.* **7** 302
[13] Cao Q *et al* 2018 A review of current development of graphene mechanics *Crystals* **8** 357
[14] Wang Y Y *et al* 2008 Raman studies of monolayer graphene: the substrate effect *J. Phys. Chem.* C **112** 10637–40

[15] Cheun Lee H, Siang-Piao Chai W-W L, Mohamed A R, Aziz C-S K A, Hidayaha N M S and Hashim U 2017 Review of the synthesis, transfer, characterization and growth mechanisms of single and multilayer graphene *R. Soc. Chem.* **7** 15644
[16] Singh S *et al* 2018 Fabrication and characterization of graphene based silicon Schottky solar cell *Superlattices Microstruct.* **120** 637–41
[17] Wan Li *et al* 2011 Electrochemistry of individual monolayer graphene sheets *Am. Chem. Soc. ACS Nano* **5** 2264–70
[18] Ferrari A C *et al* 2006 Raman spectrum of graphene and graphene layers *Phys. Rev. Lett.* **97** 187401
[19] Williams R H, Robinson G Y and Wilmsen C W 1985 *Physics and Chemistry of III-V Compound Semiconductor Interface (New York: Plenum).* ed C W Wilmsen (New York, US: Plenum Press, Springer) p 465 XIII
[20] Tung R T 1992 Electron transport of inhomogeneous Schottky barriers *Appl. Phys. Lett.* **58** 2821–23.
[21] Cheung S K, Cheung N W and Norde H 1986 Extraction of Schottky diode parameters from forward current-voltage characteristics. *Appl. Phys. Lett.* **49** 85–7
[22] Alptekin S and Altındal Ş 2019 A comparative study on current/capacitance: voltage characteristics of Au/n-Si (MS) structures with and without PVP interlayer *J. Mater. Sci., Mater. Electron.* **30** 6491–9
[23] Şenarslan E, Güzeldir B and Sağlam M 2016 Investigation of the electrical characteristics of Al/p-Si/Al Schottky diode *J. Phys. Conf. Ser.* **707** 012013
[24] Yerişkin S A, Balbaşı M and Orak İ 2017 The effects of (graphene doped-PVA) interlayer on the determinative electrical parameters of the Au/n-Si (MS) structures at room temperature *J. Mater. Sci., Mater. Electron.* **28** 14040–8
[25] Al-Dharob M H *et al* 2018 The investigation of current-conduction mechanisms (CCMs) in Au/ (0.07Zn-PVA)/n-4H-SiC (MPS) Schottky diodes (SDs) by using (*I–V–T*) measurements *Mater. Sci. Semicond. Process.* **85** 98–105
[26] Elghoul N *et al* 2015 Annealing effects on electrical and optical properties of a-Si:H layer deposited by PECVD *Mater. Sci. Semicond. Process.* **40** 302–9
[27] Cimilli Çatır F E 2018 Cu/n-InP/In schottky diyotlarin sicakliğa bağli akim-voltaj ve kapasite-voltaj ölçümlerinden elde edilen karakteristik parametrelerinin incelenmesi *Erzincan Üniv. Fen Bilimleri Enstitüsü Dergisi* (https://doi.org/10.18185/erzifbed.376279)
[28] Chand S K 1996 *J. Appl. Phys.* A **63** 171
Chand S K 1996 Current transport in Pd2Si/N-Si(100) Schottky barrier diodes at low temperatures *Appl. Phys.* A **63** 171–8
[29] Afandiyeva I M, Demirezen S and Altındal Ş 2013 Temperature dependence of forward and reverse bias current–voltage characteristics in Al–TiW–PtSi/n-Si Schottky barrier diodes with the amorphous diffusion barrier *J. Alloys Compd.* **552** 423–9
[30] Karataş Ş *et al* 2003 Temperature dependence of characteristic parameters of the H-terminated Sn/p-Si(1 0 0) Schottky contacts *Appl. Surf. Sci.* **217** 250–60
[31] Munikrishna Reddy Y *et al* 2015 Temperature-dependent electrical parameters and current transport mechanisms of Ru/Ti/n-InP Schottky diodes *Indian J. Phys.* **89** 1161–8
[32] Song Y P *et al* 1986 On the difference in apparent barrier height as obtained from capacitance–voltage and current–voltage–temperature measurements on Al/p-InP Schottky barriers *Solid-State Electron.* **29** 633–8
[33] Tung R T 2001 Recent advances in Schottky barrier concepts *Mater. Sci. Eng.* R **35** 1–138
[34] Zhu J *et al* 2018 Near unity ultraviolet absorption in graphene without patterning *Appl. Phys. Lett.* **112** 153106
[35] Paul H and Mohanta D 2011 Hydrazine reduced exfoliated graphene/graphene oxide layers and magnetoconductance measurements of Ge-supported graphene layers *Appl. Phys.* A **103** 395–402
[36] Fan Y S *et al* 2017 Monolayer-graphene-based perfect absorption structures in the near infrared *Opt. Express* **25** 13079–86